WIRELESS COMMUNICATIONS AND MOBILE COMPUTING
Wirel. Commun. Mob. Comput. 2016; **16**:1414–1430
Published online 30 June 2016 in Wiley Online Library (wileyonlinelibrary.com). DOI: 10.1002/wcm.2705

SPECIAL ISSUE PAPER

A context-aware cognitive SIMO transceiver for enhanced throughput on the downlink of LTE HetNet†

Imen Mrissa*, Faouzi Bellili, Sofiène Affes and Alex Stéphenne

INRS-EMT, Montreal, Quebec, H5A 1K6, Canada

ABSTRACT

In this paper, we design a new single-input multiple-output context-aware cognitive transceiver (CTR) that is able to switch to the best performing modem in terms of link-level throughput. On the top of conventional adaptive modulation and coding, we allow the proposed CTR to make best selection between three different pilot-utilization modes: conventional data-aided (DA) or pilot-assisted, non-DA (NDA) or blind, and NDA with pilots, which is a newly proposed hybrid version between the DA and NDA modes. We also enable the CTR to make best selection between two different channel identification schemes: conventional least-squares (LS) and newly developed maximum-likelihood estimators. Depending on whether pilot symbols can be exploited or not at the receiver, we further enable the CTR to make the best selection among two data detection modes: coherent or differential. Owing to exhaustive link-level simulations on the downlink of a long-term evolution system, we draw out the optimal decision rules in terms of the best combination triplet of pilot-use, channel-identification, and data-detection modes that yield the best link-level throughput as function of channel type, mobile speed, signal-to-noise ratio, and channel quality indicator. The proposed CTR offers a link-level throughput gains improvement as high as 700% compared with DA LS for VehB channel type at a mobile speed of 100 km/h in the low signal-to-noise ratio region. For VehA channels, its throughput gain improvements can reach 114%. For PedA and PedB channels, the proposed CTR provides throughput enhancements of about 66% and 330%, respectively. Moreover, realistic simulations at the system-level of the long-term evolution-HetNet network suggest that the new context-aware CTR outperforms the conventional transceiver (i.e., pilot-assisted LS-type channel estimation with coherent detection) by as much as 50% and 60% gains in average and cell-edge (i.e., five percentile) throughputs, respectively, in the high-clustering case with type-B channels. In the low clustering scenario, the average and cell-edge throughput gain improvements offered by the proposed CTR exceed 80% and 90% for type-B channels.

KEYWORDS

cognitive transceivers; LS and ML channel estimators; data-aided and non-data-aided detection; coherent and differential modulations; LTE; HetNet; link; and system-level simulations

***Correspondence**

Imen Mrissa, INRS-EMT, 800 De La Gauchetiere Ouest, Suite 6900, Montreal, Quebec, H5A 1K6, Canada.
E-mail: mrissa@emt.inrs.ca

1. INTRODUCTION

One of the strongest driving forces for wireless technology evolution today is 4G (4th Generation), also known as LTE-Advanced (Long Term Evolution) or IMT-Advanced (International Mobile Telecommunications) [2]. 4G allows high-speed wireless data delivery at much lower costs and latency while providing much higher rates, spectrum efficiency, and coverage. Most importantly, it promises the provision of future high-speed wireless data services everywhere closer to the mobile user in a seamless and versatile fashion, no matter what the surrounding environment and link conditions are. This stringent requirement calls for the development of new cognitive transceivers that are capable of promptly and properly self-adapting to variable operating conditions in order to constantly maximize their performance.

It is precisely in this vibrant research context that we get onto the emerging cognitive radio [3,4] from a rather uncommon perspective today. Indeed, cognitive radio is reduced in most recent works to one of its two primary

† A previous version of this paper was invited and presented in the International Conference on Wireless Communications and Mobile Computing (IWCMC) 2015 [1]. In this paper, we extend our experimental assessments to both frequency-selective channels and low-clustering scenarios.

objectives: exploit efficiently the radio spectrum with dynamic spectrum access (DSA) that allocates the least occupied frequencies, though licensed and reserved, to secondary users who are short of bandwidth [5–7]. Here, we take up its second primary objective of providing highly reliable communications anywhere anytime, so far addressed in a conventional manner, but rarely tackled today from a new level of "cognitive wireless communications" [4] where cognition could possibly handle many dynamic reconfiguration dimensions other than spectrum allocation, the conventional one. In this context, we develop in this paper a new context-aware cognitive transceiver (CTR) that is able to self-adjust its antenna-array processing structure and air-interface configuration for optimum performance. More specifically, the proposed CTR is able to select the best combination triplet of pilot-use, channel-identification, and data-detection modes that achieve the best link-level performances against channel conditions in terms of channel type, mobile speed, signal-to-noise ratio (SNR), and channel quality indicator (CQI).

Many recent research works have tackled the problem of channel estimation for LTE systems with the ultimate goal of improving coherent detection. For instance, optimizing the pilot symbols pattern was considered in [8] and [9]. Exploiting channel correlations in the time and frequency domains to enhance channel estimation in OFDM systems was also proposed in [10]. Reducing the computational complexity of the MMSE channel estimation algorithm in the LTE standard was also considered in [11]. As a matter of fact, periodic transmission of known symbols, according to a predefined and static insertion rate, is assumed by the aforementioned channel estimation algorithms as they are designed for coherent detection receivers. Yet in order to maximize the system throughput, the required pilot insertion rate and the choice of the appropriate channel estimation scheme can be optimized depending on user mobility. In fact, if the channel is assumed to be locally constant for low-mobility users, it can be accurately estimated from pilot observations only, by applying, for instance, the conventional data-aided (DA) least-squares (LS) estimator, and then used to decode the data at non-pilot observations. For high mobility users,[‡] however, the channel varies appreciably between consecutive pilot positions and increasing the number of pilots in order to track its variations leads to unacceptably high overheads. In this situation, by trading computational complexity for spectral efficiency, more sophisticated channel estimation approaches that are able to exploit observations at both pilot and non-pilot positions can be envisaged.

Motivated by these facts, we develop in this paper a cognitive transceiver that switches to the best performing channel identification algorithm between LS and maximum-likelihood (ML), and the best estimation mode between DA, NDA, and non-DA (NDA) with pilots. In fact, on the top of the conventional LS estimator, we integrate the very recent ML algorithm [12] that is tailored specifically toward time-varying SIMO channels. Moreover, the latter is able to handle the three aforementioned estimation modes on the top of its capabilities to track fast time variations with user velocities reaching 500 km/h. The underlying ML estimator is based on a piece-wise polynomial-in-time expansion for the channel involving very few unknown coefficients. In the DA scenario where the receiver has access to a pilot sequence, the DA estimator is derived in closed form. In the NDA case, however, the ML estimates for the unknown channel's polynomial approximation coefficients are retrieved iteratively using the expectation-maximization concept and the algorithm converges within few iterations.

The performance of the proposed context-aware CTR is assessed by conducting exhaustive simulations at both the link and system levels. For link-level assessment purposes, we simulate a wireless system consisting of one user equipment (UE) and one base-station (BS). We first identify the performance pertaining to each couple of {channel estimator (LS or ML), data detection (DA, NDA, or NDA with pilots)} apart and draw out the optimal decision rules in terms of the best performing {channel estimator, detection mode} configuration. Block error rate (BLER) versus SNR results are then fed to a system-level simulator, wherein a whole network is simulated in order to assess the performance of the proposed CTR under more realistic operating conditions that account for inter-cell and intra-cell interference sources. Link-level simulations reveal that the proposed cognition concept offers throughput gains in almost all operating conditions up to as much as 700% against to the conventional non-cognitive transceiver that constantly relies on the pilot-assisted LS channel estimator with coherent detection. System-level simulation results also suggest that the new context-aware CTR offers performance gains as high as 80% and 90% in terms of average and cell-edge (i.e., five percentile) throughputs, respectively.

The remainder of this paper is structured as follows. In Section 2, we introduce the context-aware CTR modes along with the different channel estimation schemes. In Section 3, link-level and system-level simulations results are presented and discussed in order to illustrate the tremendous performance gains offered by the proposed CTR. Finally, concluding remarks are drawn out in Section 4.

In the sequel, some of the common notations will be used. In fact, vectors and matrices are represented in lower-case and upper-case bold fonts, respectively. Besides, $\{.\}^{-1}$, $\{.\}^{T}$, and $\{.\}^{\dagger}$ represent the inverse, the transpose, and the Hermitian (transpose conjugate) operators, respectively. We will also denote the probability mass function (PMF) for discrete random variables by $P[.]$ and the pdf for continuous random variables by $p(.)$. The statistical expectation with respect to any random variable is denoted as

[‡]Current and future generation multi-antenna systems such as LTE, LTE-A, and beyond (LTE-B) are indeed expected to support reliable communications at very high velocities reaching 500 Km/h (e.g., high-speed trains).

$E\{.\}$. Furthermore, the operators $\Re\{.\}$, $\{.\}^*$ and $|.|$ return the real part of any complex number, its conjugate, and its amplitude, respectively.

2. CONTEXT-AWARE COGNITIVE TRANSCEIVER MODES

2.1. Data-aided or pilot-assisted mode

Pilot symbols are reference (i.e., known) symbols inserted according to a predefined mapping to be used by the receiver for channel estimation and synchronization purposes. The LTE DL pilot mapping is depicted in Figure 1. An LTE link-level SIMO transceiver block diagram with DA channel estimation is also shown in Figure 2 for antenna array configuration with N_r receiving antenna elements. A brief description of each module is provided hereafter:

- **Turbo Coding**: Introduces redundancy in the sources' binary data sequence to mitigate channel errors. The coding rate is selected according to the Channel Quality Indicator (CQI) as described in Table I.
- **Scrambling**: Interleaves code bits (we use the scrambler described in [13]).
- **QAM modulation**: Maps the code binary sequence to complex symbols.
- **OFDM symbol assembly**: Maps symbols to a time-frequency grid of size $N_{\text{freq}} \times N_{\text{symb}}$.
- **Zero Padding, Cycling prefix, and IFFT**: Zero padding consists in adding $N_{\text{IFFT}} - N_{\text{freq}}$ zeros to the signal, cycling Prefix consists in prefixing each OFDM symbol with a portion of its tail whose size must be greater or equal to the duration of the multipath delay spread. It can be configured to *normal* with durations of 5.2 and 4.7 μs for the first and remaining OFDM symbols, respectively, or to *extended* with a duration of 16.7 μs for all OFDM symbols. We opt for

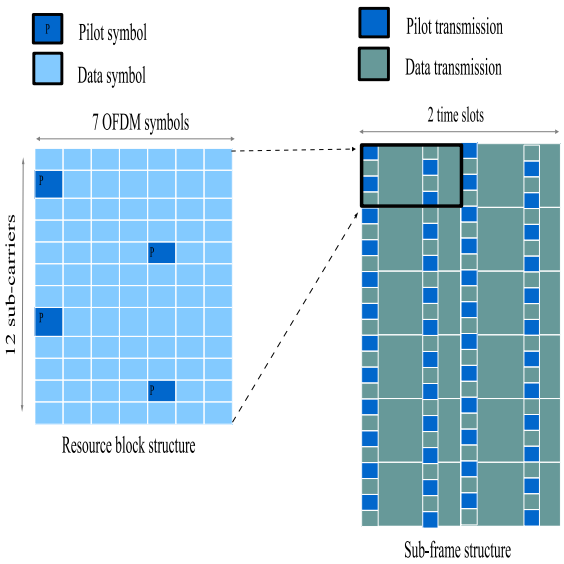

Figure 1. Long-term evolution downlink pilot mapping.

Table I. AMC schemes used by LTE downlink simulator.

CQI-C\CQI-D	Modulation	Coding rate
1	QPSK\DQPSK	0.0762
2	QPSK\DQPSK	0.1172
3	QPSK\DQPSK	0.1885
4	QPSK\DQPSK	0.3008
5	QPSK\DQPSK	0.4385
6	QPSK\DQPSK	0.5879
7	16QAM\D16StarQAM	0.3691
8	16QAM\D16StarQAM	0.4785
9	16QAM\D16StarQAM	0.6016
10	64QAM\D64StarQAM	0.4551
11	64QAM\D64StarQAM	0.5537
12	64QAM\D64StarQAM	0.6504
13	64QAM\D64StarQAM	0.7539
14	64QAM\D64StarQAM	0.8525
15	64QAM\D64StarQAM	0.9258

AMC, adaptive modulation and coding; LTE, long-term evolution.

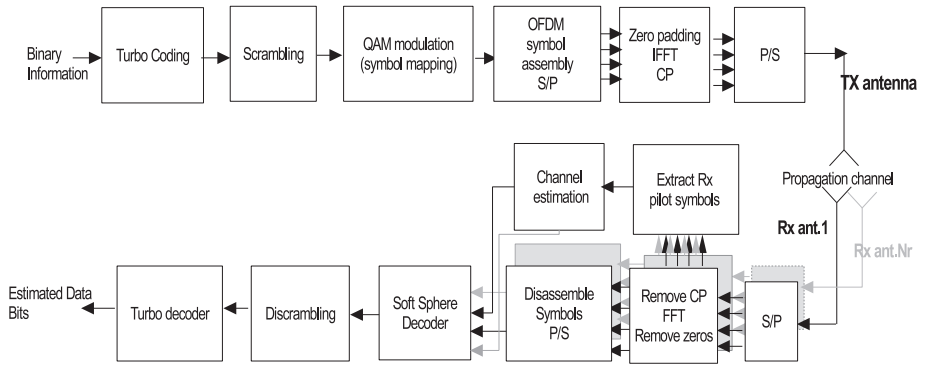

Figure 2. Block diagram of an long-term evolution downlink link-level single-input multiple-output transceiver with data-aided channel estimation.

normal cyclic prefix in our simulations. IFFT is the inverse fast Fourier transform modulating the signal before transmission.

- **Soft Sphere Decoder**: The sphere decoder extracts soft bit decisions from the received signal, y, given the channel estimate $\widehat{h}$. The soft sphere decoder computes the following log-likelihood ratios (LLRs):

$$L_b = \log\left(\frac{P\left[x_b = +1 \mid y, \widehat{h}\right]}{P\left[x_b = -1 \mid y, \widehat{h}\right]}\right), \quad b = 1, 2, \ldots, Q \tag{1}$$

  where x_b is the b^{th} bit among the Q bits of each transmitted symbol.
- **Hard bit decision**: Having the soft bit decision from the sphere decoder, this module decides of the binary transmitted bit.
- **Channel estimation**: We use either the conventional LS or the newly proposed ML channel estimator described later.

2.1.1. Least-squares channel estimator.

The LS channel estimates are obtained by minimizing the squared difference between the vector of received samples and the known pilot symbols. Let $y_{i,\mathrm{DA}}(q)$ denote the received signal (at the output of the DFT block) on pilot subcarrier i among N_{pilot} pilot subcarriers at the OFDM (pilot) symbol of index q. For convenience, we will henceforth omit the time index q. The transmitted pilot symbol, $x_{i,\mathrm{DA}}$, is related to $y_{i,\mathrm{DA}}$ as follows:

$$y_{i,\mathrm{DA}} = h_i x_{i,\mathrm{DA}} + w_i \qquad i = 0, 1, \ldots, N_{\mathrm{pilot}} - 1 \tag{2}$$

where h_i is the frequency-domain complex channel coefficient and w_i is a zero-mean Gaussian noise. The matrix notation of (2) is

$$\mathbf{y}_{\mathrm{DA}} = \mathbf{X}_{\mathrm{DA}}\mathbf{h} + \mathbf{w} \tag{3}$$

where $\mathbf{X}_{\mathrm{DA}} = \mathrm{diag}\left\{x_{0,\mathrm{DA}}, x_{1,\mathrm{DA}}, \ldots, x_{N_{\mathrm{pilot}}-1,\mathrm{DA}}\right\}$, $\mathbf{h} = \left[h_0, h_1, \ldots, h_{N_{\mathrm{pilot}}-1}\right]^T$, and $\mathbf{w} = \left[w_0, w_1, \ldots, w_{N_{\mathrm{pilot}}-1}\right]^T$. The LS algorithm minimizes $(\mathbf{y}_{\mathrm{DA}} - \mathbf{X}_{\mathrm{DA}}\mathbf{h})^{\dagger}(\mathbf{y}_{\mathrm{DA}} - \mathbf{X}_{\mathrm{DA}}\mathbf{h})$ to estimate the channel frequency response at pilot positions thereby leading to [14]:

$$\widehat{\mathbf{h}}_{\mathrm{LS}} = \mathbf{X}_{\mathrm{DA}}^{-1}\mathbf{y}_{\mathrm{DA}} \tag{4}$$

The estimates for the channel coefficients at non-pilot subcarriers are then obtained by interpolation [15]. However, when the channel is fast fading (i.e., high velocity), the underlying pilot symbols' spacing may not be sufficient for accurate tracking of the channel time variations. Note here that decreasing pilot spacing increases pilot overhead thereby limiting the effective throughput, which is not desirable for any communication system.

2.1.2. Maximum-likelihood channel estimator.

Here, we capitalize on the ML channel estimator introduced recently in [12]. Over consecutive OFDM symbols, the DA ML estimator captures the channel's time variations via a polynomial-in-time expansion of order $(J-1)$. In fact, the frequency-domain channel over each $\{r^{th}\}_{r=1}^{N_r}$ antenna branch and i^{th} subcarrier can be modeled as follows [16]:

$$h_{i,r}(t_n) = \sum_{j=0}^{J-1} c_{i,r}^{(j)} t_n^j + \mathrm{REM}_J^{(i,r)}(t_n) \tag{5}$$

where $t_n = nT_s$ with T_s being the OFDM symbol period. The polynomial order $J-1$ is a Doppler-dependent parameter optimized in [12]. Moreover, $c_{i,r}^{(j)}$ is the j^{th} coefficient of the underlying channel polynomial approximation over the i^{th} subcarrier and the r^{th} antenna element. The remainder of the Taylor series expansion, $\mathrm{REM}_J^{(i,r)}(t_n)$, can be driven to zero by dividing the whole observation window into multiple local approximation windows of sufficiently small sizes. Therefore, the channel can be locally approximated as follows [12]:

$$h_{i,r}(t_n) = \sum_{j=0}^{J-1} c_{i,r}^{(j)} t_n^j \tag{6}$$

In our simulations, ML channel estimation is performed independently over each pilot subcarrier. For the sake of simplicity, we also omit the subcarrier index in the remainder of this paper because the very same estimation procedure applies for all subcarriers.

To use a small J in (5) and avoid costly inversions of large-size matrices, the new DA ML estimator partitions the whole observation window into K local approximation windows of the same size. Let $\mathbf{c}_{k,r} = \left[c_{k,r}^{(0)}, c_{k,r}^{(1)}, \ldots, c_{k,r}^{(J-1)}\right]^T$ and $\mathbf{y}_{r,\mathrm{DA}}^{(k)} = \left[y_r^{(k)}(t_1)\, y_r^{(k)}(t_2) \ldots y_r^{(k)}\left(t_{P_{\mathrm{DA}}}\right)\right]$ be, respectively, the vectors that contain the J unknown polynomial coefficients and the P_{DA} received pilot samples[§] corresponding to the r^{th} antenna over the k^{th} approximation window. Then, by denoting $\mathbf{c}_k = \left[\mathbf{c}_{k,1}^T, \mathbf{c}_{k,2}^T, \ldots, \mathbf{c}_{k,N_r}^T\right]^T$ and $\mathbf{y}_{\mathrm{DA}}^{(k)} = \left[\mathbf{y}_{1,\mathrm{DA}}^{(k)}\, \mathbf{y}_{2,\mathrm{DA}}^{(k)} \cdots \mathbf{y}_{N_r,\mathrm{DA}}^{(k)}\right]^T$, the ML estimator maximizes the probability density function (pdf) of $\mathbf{y}_{\mathrm{DA}}^{(k)}$, parametrized by $\mathbf{c}_k$ as follows:

$$p\left(\mathbf{y}_{\mathrm{DA}}^{(k)}; \mathbf{c}_k \mid \mathbf{B}_k\right) = \frac{1}{(2\pi\sigma^2)^{N_{\mathrm{DA}}N_r}} \times \exp\left\{-\frac{1}{2\sigma^2}\left[\mathbf{y}_{\mathrm{DA}}^{(k)} - \mathbf{B}_k\mathbf{c}_k\right]^{\dagger}\left[\mathbf{y}_{\mathrm{DA}}^{(k)} - \mathbf{B}_k\mathbf{c}_k\right]\right\} \tag{7}$$

[§]Note here that P_{DA} is the number of pilot positions within each approximation window covering N_{DA} pilot and non-pilot received samples. The approximation window size N_{DA} is another Doppler-dependent design parameter optimized in [12].

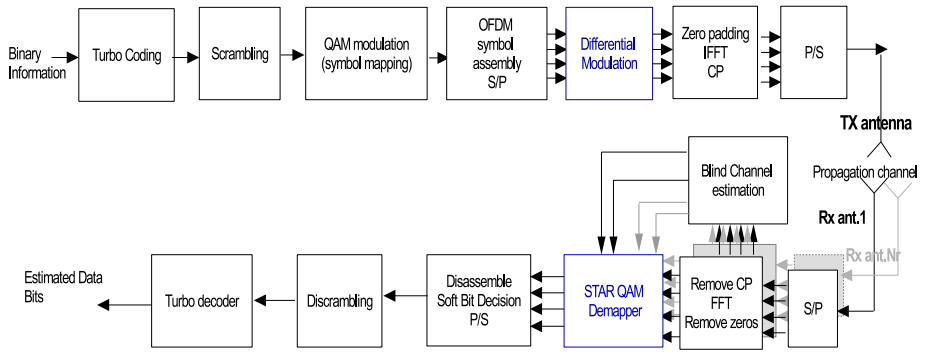

Figure 3. Block diagram of long-term evolution downlink link-level single-input multiple-output transceiver for non-data-aided channel estimation.

where $\mathbf{B}_k$ is a $P_{\mathrm{DA}}N_r \times JN_r$ block-diagonal matrix defined as $\mathbf{B}_k = \mathrm{blkdiag}\{\mathbf{A}_k\mathbf{T}, \mathbf{A}_k\mathbf{T}, \ldots, \mathbf{A}_k\mathbf{T}\}$. Here, $\mathbf{A}_k$ is the $P_{\mathrm{DA}} \times P_{\mathrm{DA}}$ diagonal matrix containing the pilot symbols covered by the k^{th} approximation window, that is, $\mathbf{A}_k = \mathrm{diag}\left\{a_k(t_1), a_k(t_2), \ldots, a_k\left(t_{P_{\mathrm{DA}}}\right)\right\}$, and $\mathbf{T}$ is a Vandermonde matrix given by the following:

$$\mathbf{T} = \begin{pmatrix} 1 & t_1 & \ldots & t_1^{J-1} \\ 1 & t_2 & \ldots & t_2^{J-1} \\ \vdots & \vdots & \ddots & \vdots \\ 1 & t_{P_{DA}} & \ldots & t_{P_{DA}}^{J-1} \end{pmatrix} \tag{8}$$

The estimates of the polynomial coefficients over all the receiving antenna branches are obtained by setting the partial derivative of the natural logarithm of $p\left(\mathbf{y}_{\mathrm{DA}}^{(k)}; \mathbf{c}_k \mid \mathbf{B}_k\right)$ in (7) to zero thereby leading to the following:

$$\widehat{\mathbf{c}}_{k,\mathrm{DA}} = \left(\mathbf{B}_k^{\dagger}\mathbf{B}_k\right)^{-1}\mathbf{B}_k^{\dagger}\mathbf{y}_{\mathrm{DA}}^{(k)} \tag{9}$$

The DA ML estimates for the channel coefficients, at both pilot and non-pilot positions, are obtained by injecting $\widehat{\mathbf{c}}_{k,\mathrm{DA}}$ in (9) back into (5).

2.2. Non-data-aided with pilots or hybrid mode

Ensuring reliable communications is the purpose of all wireless communication systems. However, user mobility and surrounding scatters' motion make accurate estimation of highly time-varying channels a truly challenging task. In fact, relying solely on pilot symbols that are often inserted far apart, in the time-frequency grid, do not enable accurate tracking of fast-varying channels. Samples received at non-pilot positions are also exploited hereafter in a hybrid channel identification scheme in order to enhance the system's performance.

2.2.1. Recursive Least Squares (RLS) channel estimator.

The hybrid mode of the LS channel estimator (using only pilot symbols to estimate the channel) is the RLS algorithm that relies on both data and pilot symbols to track the channel. The algorithm recursively estimates the channel polynomial approximation coefficients defined in (5). In fact, stacking the channel coefficients (across all the antennas) at the p^{th} OFDM symbol and subcarrier i in the vector $\mathbf{h}_p = \left[h_{i,1}(pT_s), h_{i,2}(pT_s), \ldots, h_{i,N_r}(pT_s)\right]^T$, it follows from (6) that

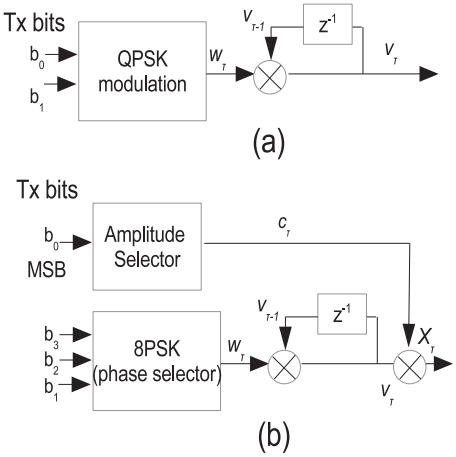

Figure 4. Differential modulation block diagram for: (a) QPSK, and (b) 16 QAM ($_\tau$ is a time (or frequency) index for time (or frequency) differential modulation.

$$\mathbf{h}_p = \mathbf{C}\mathbf{v}_p \tag{10}$$

where $\mathbf{v}_p = [1, p, \ldots, p^{J-1}]^T$ and $\mathbf{C}$ is a matrix that contains the polynomial approximation coefficients over all the antenna branches (normalized by T_s), that is,

$$\mathbf{C} = \left[\tilde{\mathbf{c}}_{i,1}, \tilde{\mathbf{c}}_{i,2}, \ldots \tilde{\mathbf{c}}_{i,N_r}\right]^T \tag{11}$$

where $\tilde{\mathbf{c}}_{i,r} = \left[\tilde{c}_{i,r}^{(0)}, \tilde{c}_{i,r}^{(1)}, \ldots, \tilde{c}_{i,r}^{(J-1)}\right]^T$ and $\tilde{c}_{i,r}^{(j)} = c_{i,r}^{(j)}T_s^j$. Note here that for ease of exposition, we drop the subcarrier index i because the same procedure is used for all subcarrires. At OFDM symbol $p+1$, the previous detected symbols are used as a training sequence of p symbols. In fact, given the previous detected symbols $\{x_{p'}\}_{p'=1}^{p}$ and

the corresponding received vectors, $\{\mathbf{y}_{p'}\}_{p'=1}^{p} \in \mathbb{C}^{N_r \times 1}$, over all the antenna branches, the polynomial coefficients matrix, $\mathbf{C}$, given in (11) is estimated using the weighted LS method as follows [17]:

$$\widehat{\mathbf{C}}_{p+1} = \arg \min_{\mathbf{C} \in \mathbb{C}^{N_r \times J}} \sum_{p'=1}^{p} \beta_{p'} \left\| \mathbf{y}_{p'} - \mathbf{C}\mathbf{v}_{p'} x_{p'} \right\|^2 \quad (12)$$

where $\beta_{p'}$ is the p'^{th} weighting coefficient given by $\beta_{p'} = \lambda^{p-p'}$ where $\lambda \in \mathbb{R}$ is referred to as a forgetting factor. The exponential weighted RLS algorithm is implemented as follows:

$$\begin{aligned}
\boldsymbol{\zeta}_p &= \Phi_{p-1}^{-1} \mathbf{v}_p x_p, \\
\alpha_p &= \frac{1}{\lambda + \boldsymbol{\zeta}_p^{\dagger} \mathbf{v}_p x_p}, \\
\Phi_p^{-1} &= \lambda^{-1} \Phi_{p-1}^{-1} - \lambda^{-1} \alpha_p \boldsymbol{\zeta}_p \boldsymbol{\zeta}_p^{\dagger} \\
\mathbf{e}_p &= \mathbf{y}_p - \widehat{\mathbf{C}}_p \mathbf{v}_p x_p, \\
\widehat{\mathbf{C}}_{p+1} &= \widehat{\mathbf{C}}_p + \alpha_p \mathbf{e}_p \boldsymbol{\zeta}_p^{\dagger}
\end{aligned}$$

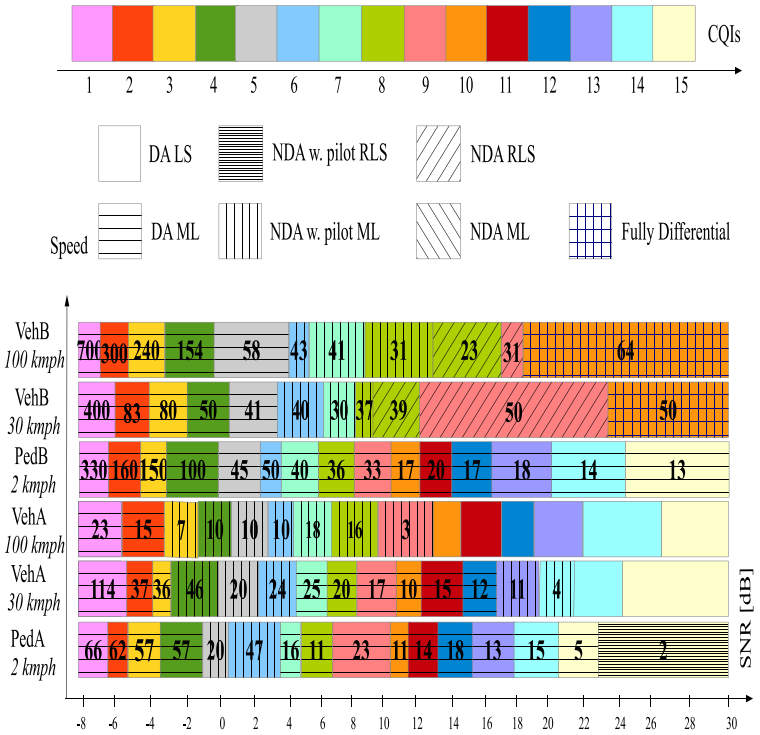

Figure 5. Decision rules of the cognitive transceiver, CTR, and the throughput gain percentages against the conventional data-aided (DA) least-squares (LS) receiver (with coherent detection) versus SNR for different channel types and mobile speeds.

Table II. Link-level simulations parameters.

Number of user equipments	1
Channel bandwidth (MHz)	15
Carrrier frequency (GHz)	2.1
Frame duration (ms)	10
Subframe duration (ms)	1
Subcarrier spacing (KHz)	15
FFT size	128
Number of subcarriers/RB	12
DL bandwidth efficiency	77.1%
OFDM symbols per subframe	14
CP length (μs)	Normal: 5.2 (first symbols) 4.69 (six following symbols)
Transmit mode	SIMO
Channel types	PedA, VehA, PedB, and VehB
Channel coding	Convolutional turbo encoder

For initialization, $\widehat{\mathbf{C}}_1$ is considered to be identically zero and Φ_0^{-1} is set to $\varrho \mathbf{I}_{(J)}$ where $\varrho \gg 1$ is a constant with sufficiently large value. Moreover, x_1 is assumed to be a pilot symbol. The estimated polynomial approximation matrix, $\widehat{\mathbf{C}}_{p+1}$, is then used in (10) along with $\mathbf{v}_{p+1}$ in order to find $\widehat{\mathbf{h}}_{p+1}$ that is required to detect the $(p+1)^{th}$ symbol x_{p+1}.

2.2.2. Maximum-likelihood channel estimator.

We consider the expectation maximization (EM)-based ML channel estimator recently introduced in [12]. This new estimator jointly exploits both pilot and data symbols to track the channel variations. In a first step, we apply over each given subcarrier the ML channel estimator that relies on pilot observations only, as described previously in Section 2.1.2, in order to find initial estimates for the channel coefficients at both pilot and non-pilot positions. In a second step, we apply the EM algorithm over all the received samples (i.e., pilots and non-pilots) in order to jointly estimate the channel coefficients and detect the unknown data symbols. The iterative EM-based algorithm runs in two main steps and uses as initialization $\widehat{\mathbf{c}}_{k,\mathrm{DA}}$ obtained in (9) from pilot positions only.

- Expectation step (E-Step):
  During the E-Step, the pdf defined in (7) takes into account all the possible transmitted symbols $\{a_m\}_{m=1}^{M}$ where M is the modulation order. In fact, at each EM iteration l, and within each k^{th} approximation window (of size N_{NDA} symbols), the objective function is updated as follows:

$$Q\left(\mathbf{c}_k \mid \widehat{\mathbf{c}}_k^{(l-1)}\right) = -N_{\mathrm{NDA}} N_r \ln(2\pi\sigma^2) - \frac{1}{2\sigma 2}\sum_{r=1}^{N_r} \times \left(M_{2,k}^{(r)} + \sum_{n=1}^{N_{\mathrm{NDA}}} \alpha_{n,k}^{(l-1)} \left|\mathbf{c}_{r,k}^T \mathbf{t}(n)\right|^2 - 2\beta_{r,n,k}^{(l-1)}(\mathbf{c}_{r,k}) \right) \tag{13}$$

where $M_{2,k}^{(r)} = E\{|y_{r,k}(n)|^2\}$ is the second-order moment of the received samples over the r^{th} receiving antenna branch and $\mathbf{t}(n) = \left[1, t_n, t_n^2, \ldots, t_n^{J-1}\right]^T$. Moreover, by denoting the constellation alphabet as $\mathcal{C} = \{a_1, a_2, \ldots, a_M\}$, the other quantities involved in [12] are given by

$$\alpha_{n,k}^{(l-1)} = \sum_{m=1}^{M} P_{m,n,k}^{(l-1)} |a_m|^2 \tag{14}$$

$$\beta_{r,n,k}^{(l-1)}(\mathbf{c}_{r,k}) = \sum_{m=1}^{M} P_{m,n,k}^{(l-1)} \Re\left\{y_{r,k}^*(n) a_m \mathbf{t}(n)^T \mathbf{c}_{r,k}\right\} \tag{15}$$

Table III. Multipath power delay profile.

Channel type	Relative delay (ns)	Relative power (dB)
PedA	0	0
	110	−9.7
	190	−19.2
	410	−22.8
PedB	0	0
	200	−0.9
	800	−4.9
	1200	−8
	2300	−7.8
	3700	−23.9
VehA	0	0
	310	−1
	710	−9
	1090	−10
	1730	−15
	2510	−20
VehB	0	−2.5
	300	0
	8900	−12.8
	12900	−10
	17100	−25.2
	20000	−16

where $P_{m,n,k}^{(l-1)} = P\left(a_m \mid \mathbf{y}_k(n); \widehat{\mathbf{c}}^{(l-1)}\right)$ is the *a posteriori* probability of a_m at iteration $(l-1)$ that is computed using the Bayes' formula as follows:

$$P_{m,n,k}^{(l-1)} = \frac{P[a_m]p\left(\mathbf{y}_k(n)|a_m; \widehat{\mathbf{c}}_k^{(l-1)}\right)}{p\left(\mathbf{y}_k(n); \widehat{\mathbf{c}}_k^{(l-1)}\right)} \tag{16}$$

Since the transmitted symbols are assumed to be equally likely, we have $P(a_m) = \frac{1}{M}$ and therefore:

$$p\left(\mathbf{y}_k(n); \widehat{\mathbf{c}}_k^{(l-1)}\right) = \frac{1}{M}\sum_{m=1}^{M} p\left(\mathbf{y}_k(n)|a_m; \widehat{\mathbf{c}}_k^{(l-1)}\right)$$

$$= \frac{1}{M(2\pi\sigma^2)^{N_r}}\sum_{m=1}^{M}\exp\left\{-\frac{1}{2\sigma^2}\sum_{r=1}^{N_r}\left|y_{r,k}(n) - a_m\mathbf{c}_{r,k}^T\mathbf{t}(n)\right|^2\right\} \tag{17}$$

- Maximization step (M-Step):
  During the M-Step, the objective function obtained in (13) is maximized with respect to $\mathbf{c}_k$:

$$\widehat{\mathbf{c}}_k^{(l)} = \underset{\mathbf{c}_k}{\text{argmax}}\, Q\left(\mathbf{c}_k|\widehat{\mathbf{c}}_k^{(l-1)}\right) \tag{18}$$

yielding the following more refined estimates for the polynomial approximation coefficients:

$$\widehat{\mathbf{c}}_{r,k}^{(l)} = \left(\sum_{n=1}^{N_{\text{NDA}}}\mathbf{t}(n)\mathbf{t}(n)^T\right)^{-1}\sum_{n=1}^{N_{\text{NDA}}}\lambda_{r,n,k}^{(l-1)}\mathbf{t}(n) \tag{19}$$

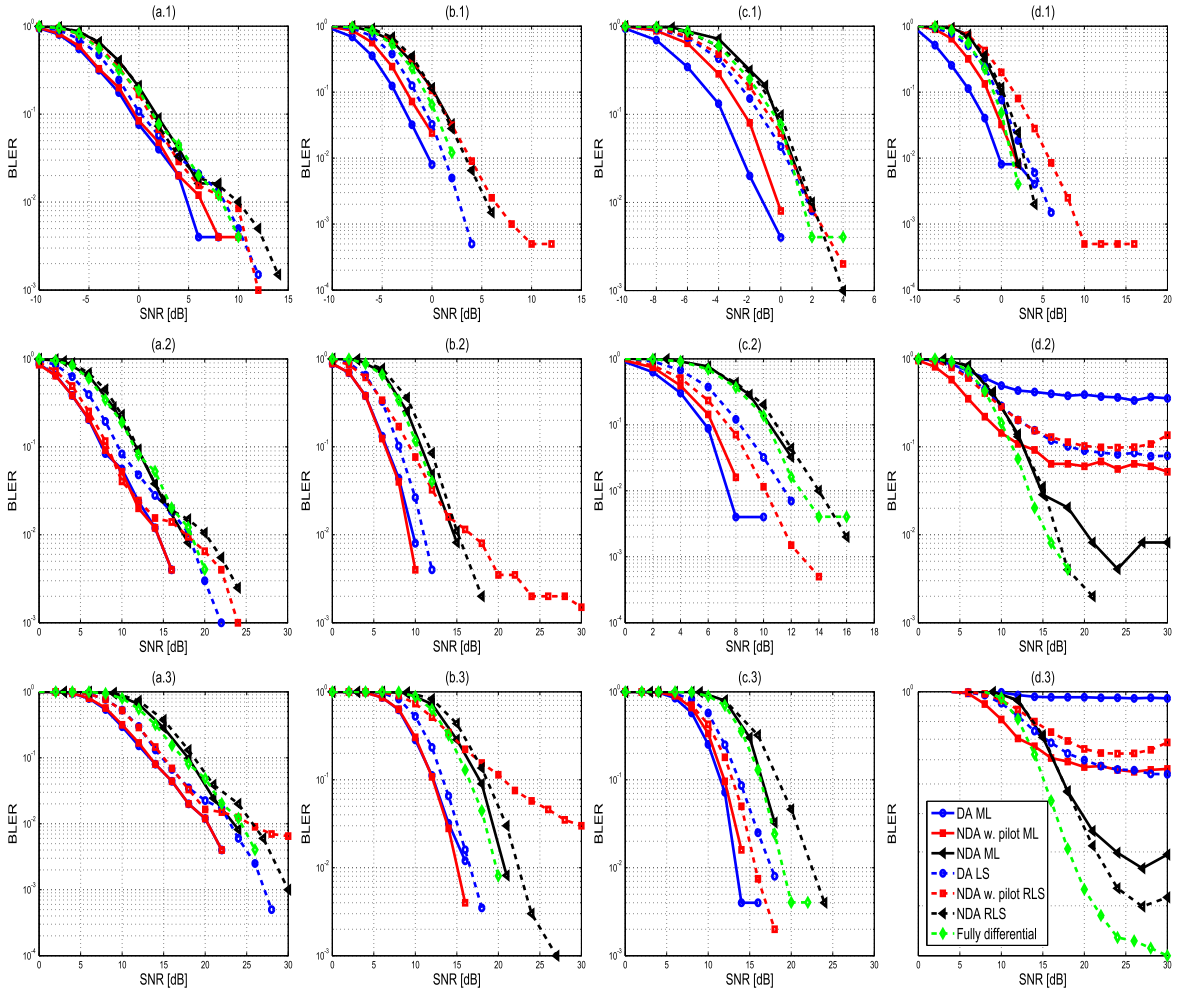

Figure 6. Block error rate curves for different channel estimation algorithms and data detection modes implemented for our CTR for different channel types and mobile speeds: a) PedA 2 km/h, b) VehA 30 km/h, c) PedB 2 km/h, and d) VehB 100 km/h; and for: 1) QPSK/CQI = 1, 2) 16QAM/CQI = 7, and 3) 64QAM CQI = 10 MCSs.

Here, $\lambda_{r,n,k}^{(l-1)}$ is given by:

$$\lambda_{r,n,k}^{(l-1)} = \left[\widehat{a}_k^{(l-1)}(t_n)\right]^* y_{r,k}(t_n) \tag{20}$$

in which

$$\widehat{a}_k^{(l-1)}(t_n) = \sum_{m=1}^{M} P_{m,n,k}^{(l-1)} a_m \tag{21}$$

is the soft symbol estimate at iteration $l-1$. Note here that the EM-based algorithm described earlier is iterative in nature and as such requires accurate initial guesses about the polynomial-approximation coefficients in order to converge to the global maximum of the Log-Likelihood function (LLF). For this reason, it is initialized using the pilot-based DA ML estimates already obtained in (9) as discussed in some depth in [12].

2.3. Non-data-aided or blind mode

For blind or NDA channel estimation, no pilot symbols are exploited by the receiver. Phase ambiguity is resolved by differential modulation. The blind RLS channel estimator algorithm is already the one described in Section 2.2.1. However, an arbitrary guess of the first transmitted symbol is used to initialize the recursive algorithm. The blind channel ML estimation algorithm is also the one described in Section 2.2.2. The only difference, however, is that the initialization is arbitrary and random. Figure 3 presents the block diagram of the SIMO transceiver with the NDA channel estimation. On the top of those already detailed in Section 2.1, the new modules are described as follows:

- **Differential modulation**: Modulates the phase difference between two consecutive transmitted symbols [18] as described in Figure 4 .
- **STAR QAM Demapper**: To fully exploit the potential power of channel coding, soft-decision based demodulation is required. For this purpose, we use the soft decision aided DAPSK detection algorithm

Table IV. System-level simulation parameters.

Macrocell parameters	
Cellular layout	Hexagonal grid, 7 cell sites with BTS in the center of the cell
Inter-site distance	500 meters
Minimum UE to macro-BS distance	35 meters
Path loss model	TS 36.942, sub-clause 4.5.2
Antenna pattern	3-dimensional TS 36.942
TX antennas	1
Shadowing	Log-normal with 10 dB standard deviation
LTE BS antenna gain after cable loss7	17 dBi
Macro BS antenna height	32 meters
Maximum macro-BS TX power	46 dBm (conventional)
MCL	70 dBm
Scheduling algorithm	Proportional Fair
Resource Block width	180 kHz
Pico-cell parameters	
Cellular layout	Circular shape with BTS in the center of cell
Minimum distance between pico pNodeBs	40 meters
Minimum distance between new node and regular nodes	75 meters
Minimum UE to pico-BS distance	10 meters
Path loss model	TS 36.942, sub-clause 4.5.2
Antenna pattern	Omnidirectional
TX antennas	1
shadowing	Log-normal with 10 dB standard deviation
Antenna gain	5 dBi
Maximum pico-DS TX power	30 dBm
Scheduling algorithm	Proportional Fair
UE parameters	
UE Rx antennas	2
UE antenna gain	0 dBi
UE noise figure	9 dB
Number of UEs per cell-site area	60

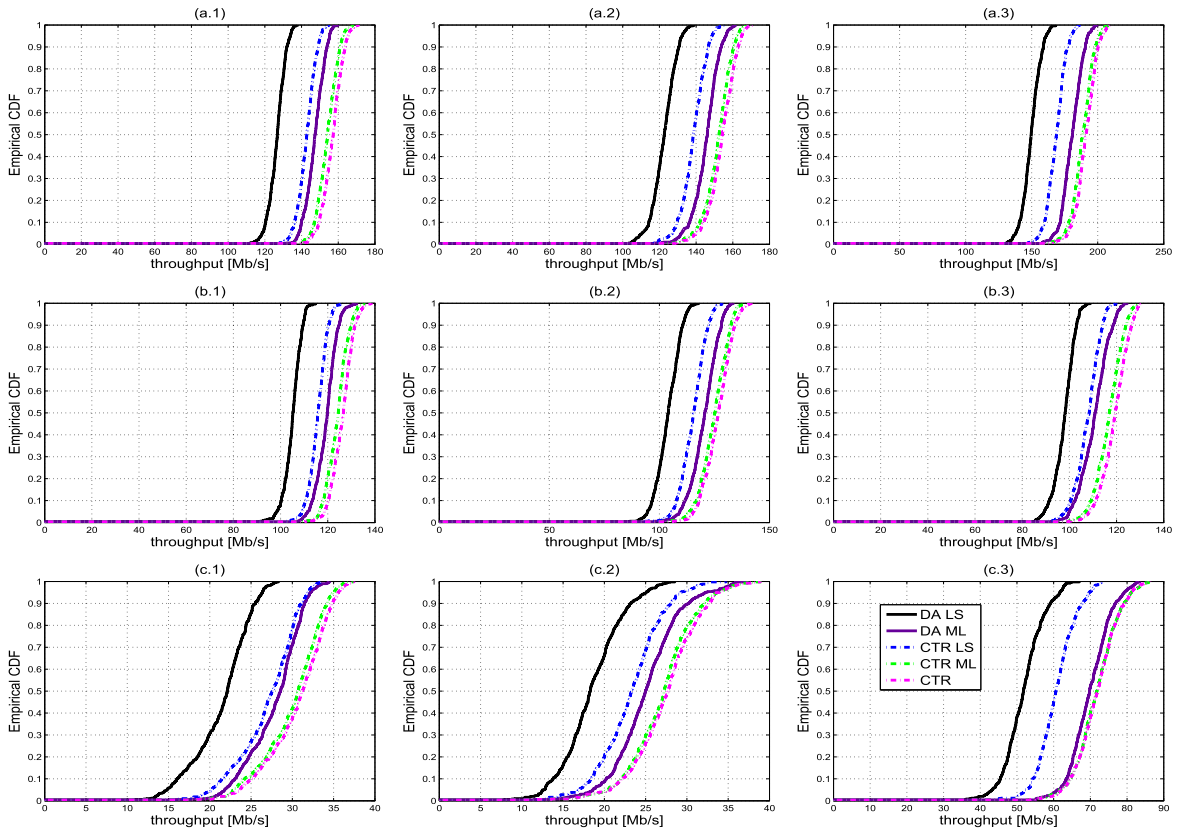

Figure 7. Long-term evolution HetNet empirical CFDs of downlink system-level throughput for (1) 1 pico-cell per macro area, (2) 2 pico-cells per macro area, and (3) 4 pico-cells per macro area; a) total cell-site, b) macro-cell, and c) pico-cell in case of low clustering over type-A channels.

developed in [19] and [20] and referred to hereafter as the STAR QAM Demapper. The *a posteriori* LLR expression used in the joint amplitude-phase detector is given by:

$$\mathrm{LLR}(b_m) = \ln\left(\frac{\sum_{s_\tau \in s_{b_m=1}} \exp\left[d(\varphi^\upsilon, \omega^l)\right]}{\sum_{s_\tau \in s_{b_m=0}} \exp\left[d(\varphi^\upsilon, \omega^l)\right]}\right) \quad (22)$$

where $s_{b_m=0}$ and $s_{b_m=1}$ represent the set of symbols went the m^{th} bit, b_m, is 0 and 1, respectively. The probability metric $d(\varphi^\upsilon, \omega^l)$ in case of fully differential version, for which no channel estimation is required, is defined as follows:

$$d(\varphi^\upsilon, \omega^l) = -\frac{\|\mathbf{y}_{\tau+1} - \varphi^\upsilon \omega^l \mathbf{y}_\tau\|^2}{\tilde{N}_0^\upsilon} \quad (23)$$

where

- $\mathbf{y}_\tau$ is the received symbol vector $\mathbf{y}_\tau = [y_{\tau,1}; \ldots; y_{\tau,N_r}]$ where τ is the time (or frequency) index in the case of time (or frequency) differential modulation.
- φ is the amplitude ratio of two consecutive transmitted symbols and $\upsilon \in [1, \ldots, 2M_A - 1]$ where M_A is the number of amplitude rings ($M_A = 1$ for DQPSK, $M_A = 2$ for D16STAR QAM, and $M_A = 4$ for D64STAR QAM).
- ω is the phase difference of two consecutive transmitted symbols and $l \in [1, .., M_p]$ where M_p is the number of phases in the DAPSK constellation.
- $\tilde{N}_0^\upsilon$ is the equivalent noise power defined as $\tilde{N}_0^\upsilon = [1 + (\varphi^\upsilon)^2] N_0$ for $\upsilon \in \{1, \ldots, 2M_A - 1\}$ where N_0 is the observation noise power.

The probability metric $d_{\mathrm{NDA}}(\varphi^\upsilon, \omega^l)$ under NDA channel estimation is given by

$$d_{\mathrm{NDA}}(\varphi^\upsilon, \omega^l) = -\frac{\left\|\mathbf{y}_{\tau+1} - \varphi^\upsilon \omega^l \hat{\mathbf{h}}_\tau \hat{x}_\tau\right\|^2}{N_0} \quad (24)$$

where $\hat{\mathbf{h}}_\tau$ is the blind estimate channel vector and $\hat{x}_\tau$ is the estimated transmitted symbol at the time (or frequency) index τ obtained by NDA RLS or NDA ML channel estimators.

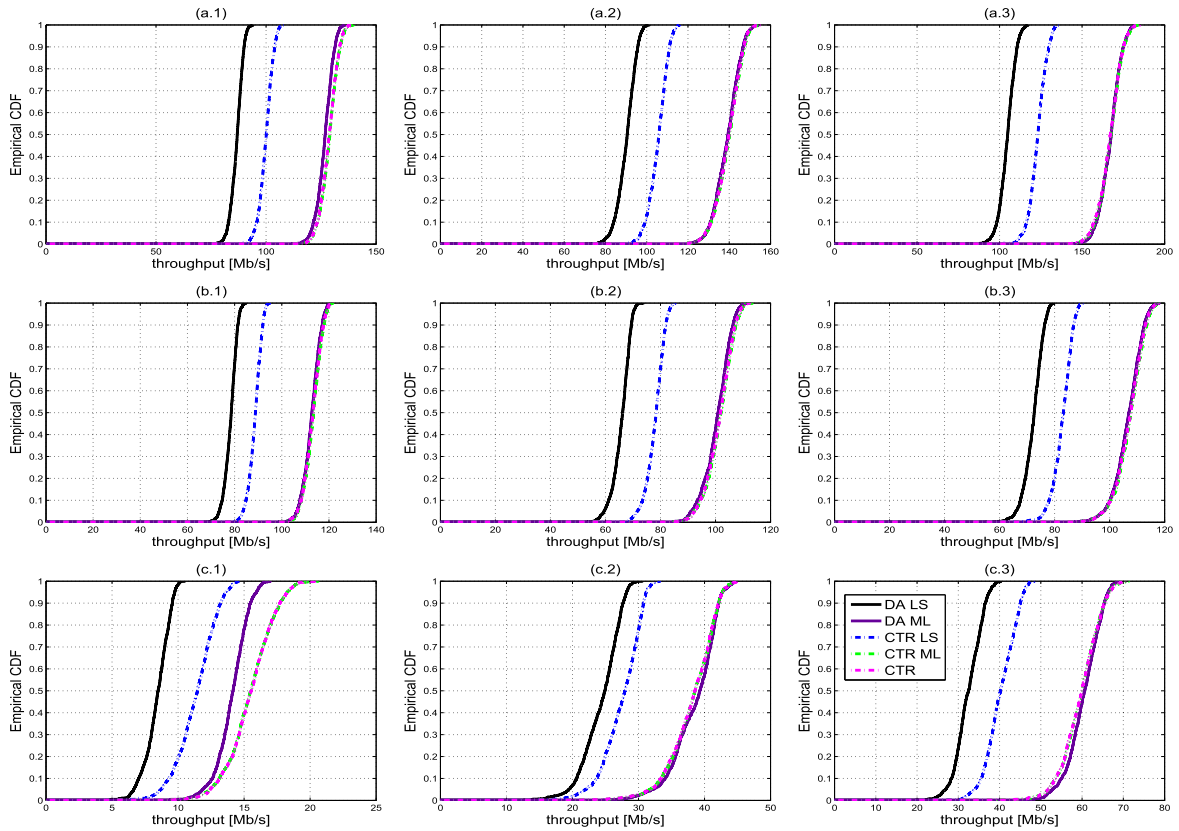

Figure 8. Long-term evolution HetNet empirical CFDs of downlink system-level throughput for (1) 1 pico-cell per macro area, (2) 2 pico-cells per macro area, and (3) 4 pico-cells per macro area; and: a) total cell-site, b) macro-cell, and c) pico-cell in the case of low clustering over type-B channels.

2.4. Data detection modes

On the top of selecting the appropriate channel estimator and pilot-use modes among DA ML, NDA w. pilot ML, NDA ML, DA LS, NDA w. pilot RLS and NDA RLS, the new context-aware CTR selects one of the following data detection schemes:

- Coherent if pilot symbols are used; or
- Non coherent or differential if no pilot symbols are used.

We also implement a "fully differential" transceiver version for which no channel estimation is required. Data detection is based on differential modulation-demodulation only as described in Equation (23). We use time differential modulation as it provides better performance than frequency differential modulation in case of frequency selective channels (type-B channels) [21,22].

3. SIMULATION SETUP AND RESULTS

A 1×2 antenna configuration (1 transmit antenna at the eNodeB and 2 receive antennas at the mobile) is considered as a SIMO configuration example for discussion in the rest of this paper. In the following, exhaustive computer simulations will be conducted in order to assess the performance of the newly proposed CTR at both the link- and system-levels.

3.1. Link-level simulations

In this section, link-level simulations assuming only one base station and a single mobile user are used to draw out decision rules regarding the following:

(1) The best channel estimation algorithm between the conventional LS and the newly proposed ML estimators.
(2) The best channel identification mode [among DA, NDA w. pilot (i.e., hybrid), and completely NDA] that yields the highest link-level throughput.
(3) The best detection scheme between coherent and differential detection depending on whether pilot symbols can be properly exploited or not at the receiver, respectively.
(4) The best modulation-coding CQI couple among the conventional coherent (CQI-C) and the newly-designed differential (CQI-D) ones (cf. Table I).

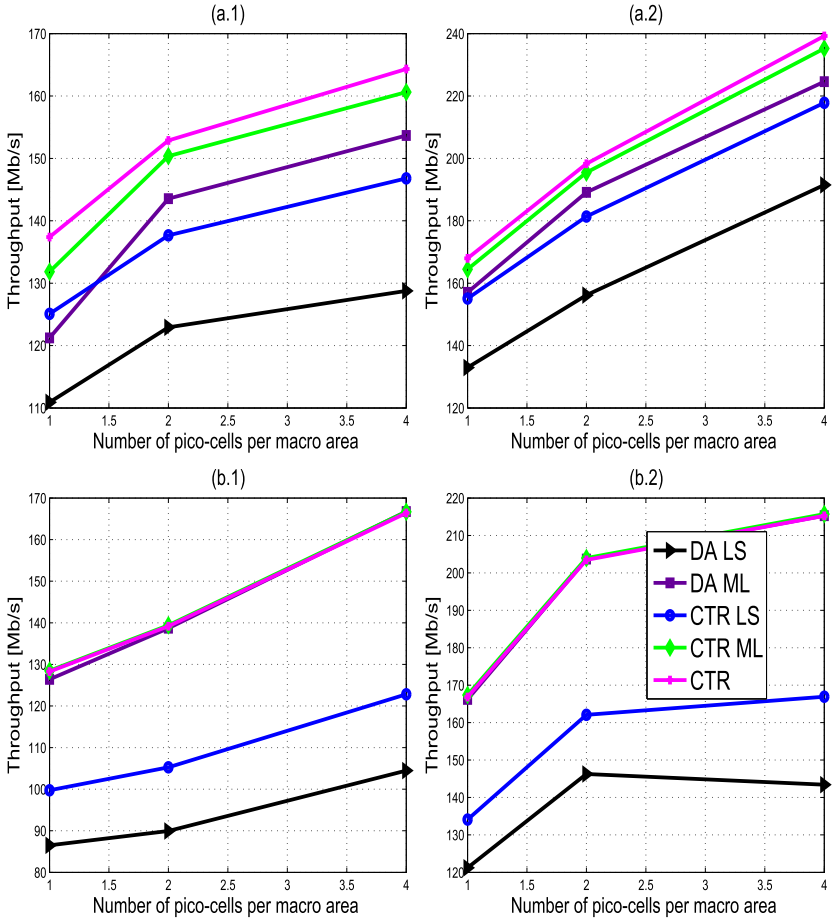

Figure 9. System-level total cell-site throughput for (1) low and (2) high clustering; and (a) type-A, and (b) type-B channels.

The CTR selects the best output quadruplet among the four processing dimensions earlier that offers the best link-level throughout performance for any given input triplet of channel conditions, that is, SNR/CQI, mobile speed, and channel type. The relationships governing the latter outputs versus inputs, referred to as decision rules, are determined in Figure 5 offline by link-level simulations in a so-called learning phase. During online operation, the CTR selects according to these decision rules the best quadruplet of processing modes that best copes in link-level throughput with the experienced triplet of operating channel conditions; actually in the same manner conventional transceivers switch today between adaptive modulation and coding schemes (MCSs) versus the SNR. From this perspective, the proposed CTR actually extends the simple conventional adaptive modulation and coding (AMC) concept to far larger dimensions, from a single input CSI parameter to three, and from a single output processing mode to four. Furthermore, the CTR online operation requires *a priori* the estimation of the SNR or SINR, the Doppler (i.e., mobile speed), and the channel type. However, the results disclosed in this paper assume perfect knowledge of these channel parameters. More elaborate simulation results that integrate the estimation of these parameters, currently under investigation, fall beyond the scope of the present work.

Most significant LTE DL link-level parameters are summarized in Table II.

We consider Pedestrian A and B (PedA and PedB) slow-fading channel models for users with a mobile speed of 2 km/h and Vehicular A (VehA) and B (VehB) for fast-fading channels for users with mobile speeds of 30 and 100 km/h, respectively. Their power delay profiles (PDPs) are given in Table III.

In order to account for adaptive modulation and coding (AMC), a CQI value indicates to the eNodeB the modulation order and the channel coding rate adopted in each subframe.

As highlighted in Table I, the CQI value ranges between 1 and 15 defining, respectively, six, three, and six possible coding rates for QPSK/DQPSK, 16QAM/D16Star-QAM, and 64QAM/D64Star-QAM modulations [23]. Note that CQI-C and CQI-D stand for coherent and differential detection modulations, respectively. In our simulations, the CQI values as well as the SNR are assumed to be perfectly known to the receiver. Assessment of CQI feedback and

delay errors are beyond the scope of this work. BLER performances results are presented in Figure 6 for different channel types and mobile speeds. As seen there, the best performing channel estimator (among LS and ML) and data detection mode (among DA, NDA and NDA with pilots) both depend on the environment conditions characterized by the channel type, mobile speed, and SNR/CQI values. Based on these results, we identify the optimal CTR's decision rules that correspond to the best channel estimation scheme and data detection mode along with the associated throughput gain for each channel condition triplet as depicted in Figure 5. We define three different CTRs depending on the implemented channel estimation algorithms. The first one (denoted hereafter as "CTR LS") switches between the fully differential detection mode and the different LS channel estimation schemes, namely, DA LS, NDA w. pilot LS, and NDA LS. The second one (referred as "CTR ML") switches between the fully differential detection mode and the different ML channel estimation schemes, namely DA ML, NDA w. pilot ML, and NDA ML. The third CTR which is a smarter cognitive transceiver (denoted hereafter simply as "CTR") is able to switch between all the detection modes and channel estimation schemes listed previously for both CTR ML and CTR LS. Figure 5 depicts the link-level throughput gains of CTR against the conventional non-cognitive transceiver that applies the DA LS channel estimator regardless of the channel conditions. The gains are presented for each triplet (channel type, mobile speed, SNR/CQI value). Note here that link-level throughput gains for CTR-LS and CTR-ML are not shown due to space limitations. Their performance will, however, be assessed later in Section 3.2. As seen from Figure 5, CTR offers tremendous link-level throughput gains over the conventional DA LS transceiver that can reach up to 700%, in the low-SNR region for VehB channels and a mobile speed of 100 km/h. For flat-fading channels (type-A channels), Figure 5 shows that the DA ML channel estimator outperforms the DA LS estimator at low mobile speeds (PedA channel). This result confirms that pilot-only channel estimation is still reliable in the case of low-speed flat-fading channels. However, for fast-fading type-A channels (VehA with 30 and 100 km/h), the NDA with pilots ML channel estimator exhibits better performance for most of the CQIs values. Figure 5 also reveals

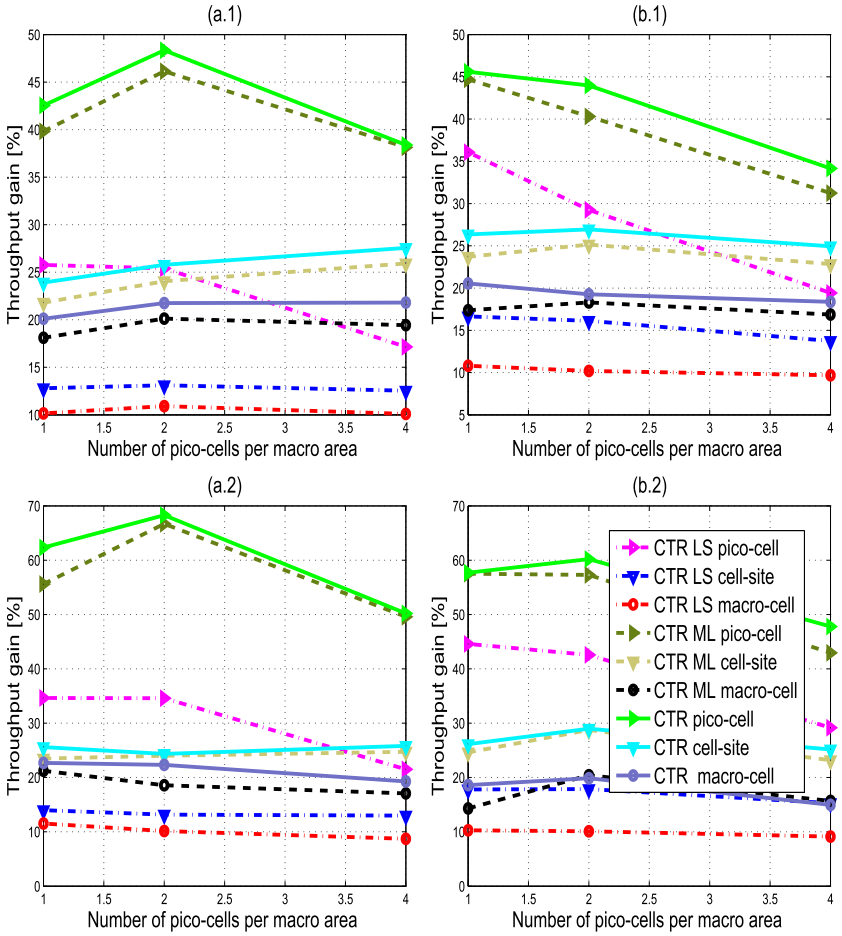

Figure 10. (1) Average and (2) cell-edge system-level throughput gains for the pico-cell, macro-cell, and the whole cell-site in the cases of: a) low, and b) high clustering over type-A channels.

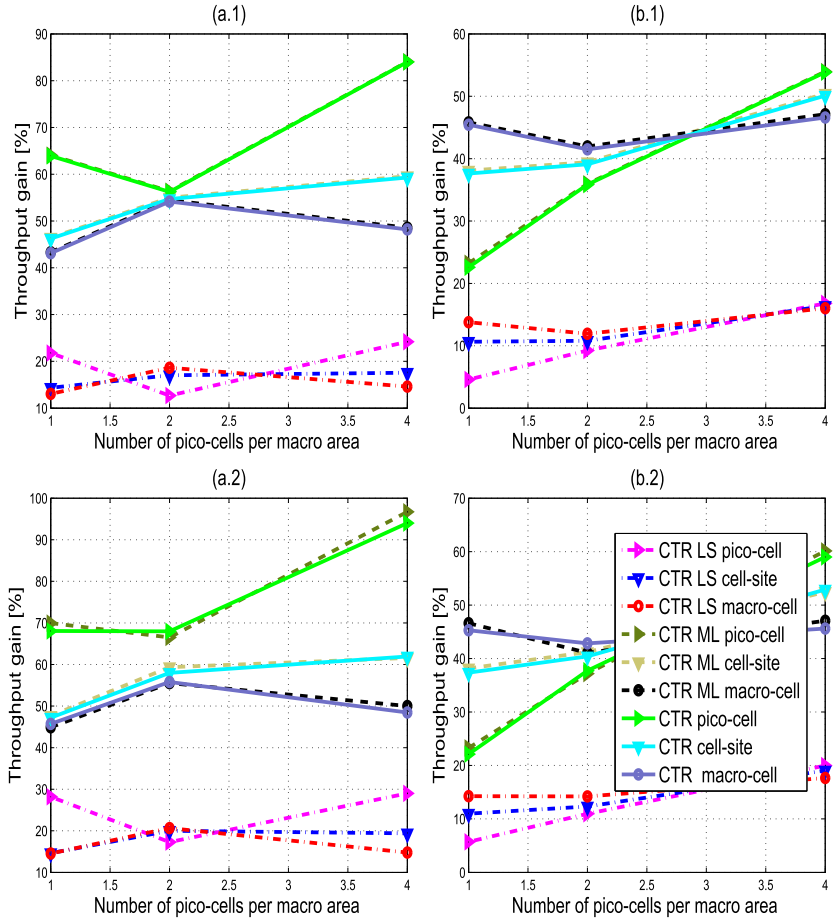

Figure 11. (1) Average and (2) cell-edge system-level throughput gains for the pico-cell, macro-cell, and the whole cell-site in the cases of: (a) low, and (b) high clustering over type-B channels.

that blind channel estimation (NDA) and differential detection outperforms the pilot-assisted channel estimators (DA and NDA with pilots) for high-order modulations over frequency-selective channels (type-B channels) at medium and high mobile speeds (VehB with 30 and 100 km/h). This fact is due to the fast channel variations along successive subcarriers which makes linear interpolation no longer reliable. At low mobile speeds (PedB channel), the newly proposed DA ML outperforms all other channel estimation algorithms and achieves a throughput gain of about 330% in the low-SNR region.

3.2. System-level simulations

The link-level-based decision rules, identified in the previous section, are then fed to a HetNet LTE DL system-level simulator wherein a whole network is simulated in order to assess the performance of the proposed CTR under more realistic operating conditions that account for inter-cell and intra-cell interference sources. More specifically, we simulate a 7-hexagonal-cell network with pico-cells dropped randomly in each macro area. An exhaustive list of the system-level parameters used in our simulations is provided in Table IV. We also assume that 50% of the users move with a speed of 2 km/h and experience PedA/PedB channel type. The remaining 30% and 20% of the users are assumed to have a speed of 30 and 100 km/h, respectively, and experience a VehA/VehB channel type. Furthermore, we consider the case of $\{1, 2, 4\}$ pico-cells in each macro area as defined in [24]. We also consider both low and high clustering distributions for the UEs. For high clustering scenario, 2/3 of UEs are dropped in the hotspots. In case of low clustering scenario, four UEs are dropped in each hotspot with other UEs are dropped uniformly over the macro-cell area (including hotspots). Hereafter, we show the simulation results for the whole cell site, the central macro-cell as well as its pico-cells. Figures 7 and 8 show system-level LTE DL throughput CDFs for DA ML, DA LS, CTR ML, CTR LS, and CTR transceivers for type-A and -B channels with low clustering[¶]. In all considered

[¶]Throughput CDFs in high clustering are not shown here due to space limitations. However, this case will be assessed later in Figures 9, 10, and 11.

cases, CTR always delivers the highest throughput with overwhelming probability among all transceivers. Figure 9 shows the impact of the number of dropped pico cells per-macro area on the different cognitive transceivers. The average DL system-level throughput increases with the number of picocells with maximum values achieved by the smartest (ML-LS-based) CTR. Figures 10 and 11, however, show the average and fifth percentile (i.e., cell-edge) DL throughput gains at the system-level over type-A and -B channels, respectively. Huge performance gains are achieved by combining the cognitive transceiver concept and the new channel estimator recently introduced in [12]. In fact, in terms of cell-site performance, CTR exhibits about 25% and 50% DL throughput gains (average and fifth percentile) over type-A and type-B channels, respectively. In terms of pico-cell performance, the fifth percentile (i.e., cell-edge) and average gains exceed 50% and 40%, respectively, in the low clustering type-A channel scenario. These gains become as high as 80% and 90% in the low clustering type-B channel scenario, respectively. Based on these results, the proposed CTR turns out to be extremely advantageous in HetNet small cells where users suffer from serious interference problem due to weak transmitted power.

4. CONCLUSION

In this paper, we developed a new SIMO context-aware transceiver that is able to switch to the best performing modem in terms of link-level throughput. On the top of conventional AMC, we allow the proposed CTR to make best selection among three different pilot-utilization modes: conventional (DA) or pilot-assisted, non-DA (NDA) or blind, and NDA with pilots which is a newly proposed hybrid version between the DA and NDA modes. We also enable the CTR to make best selection between two different channel identification schemes: conventional least-squares (LS) and newly developed ML estimators. Depending on whether pilot symbols can be properly exploited or not at the receiver, we further enable the CTR to make best selection among two data detection modes: coherent or differential. Owing to extensive and exhaustive link-level simulations on the DL of the LTE system, we were able to draw out the decision rules of the new CTR that identify the best combination triplet of pilot-use, channel-identification, and data-detection modes that deliver the best link-level throughput at any operating conditions in terms of channel type, mobile speed, SNR, and CQI. The proposed CTR offers a link-level throughput gain in almost all operating conditions up to as much as 700% against the conventional non-cognitive DA LS transceiver (i.e., pilot-assisted LS-type channel estimation with coherent detection). Realistic extensive simulations of LTE heterogeneous network (HetNet) at the system-level also suggest that the new proposed CTR outperforms the conventional DA LS transceiver by as much as 60% gains in average and cell-edge (i.e., five percentile) total throughput per macro-area. Applying our new cognition concept is hence very promising to enhance LTE HetNet network.

ACKNOWLEDGEMENTS

Work supported by the CREATE PERSWADE www.create-perswade.ca and the Discovery Grants Programs of NSERC and a Discovery Accelerator Supplement (DAS) Award from NSERC.

REFERENCES

1. Mrissa I, Bellili F, Affes S, Stéphenne A. A context-aware cognitive SIMO transceiver for increased LTE-HetNet system-level DL-throughput. In *International Conference on Wireless Communications and Mobile Computing (IWCMC) (invited paper)*, Dubrovnik, August 2015; 19–25, (Invited Paper).
2. Khan F. *LTE-Advanced for 4G Mobile Broadband Air Interface Technologies and Performance*. Cambridge University Press: New York, USA, 2009.
3. Mitola J, III. *Cognitive Radio Architecture*. John Wiley & Sons: Hoboken, New Jersey, 2006.
4. Haykin S. Cognitive radio: brain-empowered wireless communications. *IEEE Journal on Selected Areas in Communications* 2005; **3**(2): 201–220.
5. Krenik W, Wyglinski AM, Doyle LE. Cognitive radios for dynamic spectrum access. *IEEE Communications Magazine* 2007; **45**(5): 64–65.
6. Huang JW, Krishnamurthy V. Cognitive base stations in LTE/3GPP femtocells: a correlated equilibrium game-theoretic approach. *IEEE Transactions on Communications* 2011; **59**(12): 3485–3493.
7. Attar A, Krishnamurthy V, Gharehshiran ON. Interference management using cognitive base-stations for UMTS LTE. *IEEE Communications Magazine* 2011; **49**(8): 152–159.
8. Simko M, Diniz PSR, Rupp M. Design requirements of adaptive pilot-symbol patterns. In *IEEE International Conference on Communications (ICC) - Workshop Beyond LTE-A*, Budapest, June 2013; 144–148.
9. Simko M, Diniz PSR, Wang Q, Rupp M. New insights in optimal pilot symbol patterns for OFDM systems. In *IEEE Wireless Communications and Networking Conference (WCNC)*, Shanghai, April 2013; 3737–3741.
10. Al-Naffouri TY, Islam KMZ, Al-Dhahir N, Lu S. A Model reduction approach for OFDM channel estimation under high mobility conditions. *IEEE Transactions on Signal Processing* 2010; **58**(4): 2181–2193.
11. Omar S, Ancora A, Slock DTM. Performance analysis of general pilot-aided linear channel estimation in LTE OFDMA systems with application to simplified

MMSE schemes. In *IEEE 19th International Symposium on Personal Indoor and Mobile Radio Communications (PIMRC)*, Cannes, France, September 2008; 1–6.
12. Bellili F, Meftehi R, Affes S, Stéphenne A. Maximum likelihood SNR estimation of linearly-modulated signals over time-varying flat-fading SIMO channels. *IEEE Transactions on Signal Processing* 2015; **63**(2): 441–456.
13. *Evolved Universal Terrestrial Radio Access (E-UTRA); Physical Channels and Modulation*, 3GPP Standard TS 36.211, V8.2.0 (2008-03), Release 8.
14. van de Beek J, Edfors O, Sandell M, et al. On channel estimation in OFDM systems. In *IEEE 45th Vehicular Technology Conference*, Vol. 2, Chicago, July 1995; 815–819.
15. Omar S, Ancora A, Slock DTM. Performance analysis of general pilot-aided linear channel estimation in LTE OFDMA systems with application to simplified MMSE schemes. In *Proceedings of IEEE 19th International Symposium on Personal, Indoor and Mobile Radio Communications (PIMRC)*, Cannes, September 2008; 1–6.
16. Bello P. Characterization of randomly time-variant linear channels. *IEEE Transactions on Communications Systems* 1963; **11**(4): 360–393.
17. Haykin S. *Adaptive Filter Theory* (3rd edn). Prentice Hall: Hamilton, Ontario, Canada, 1996.
18. May T, Rohling H, Engels V. Performance analysis of Viterbi decoding for 64-DAPSK and 64-QAM modulated OFDM signals. *IEEE Transactions on Communications* 1998; **46**(2): 182–190.
19. Liang D, Ng SX, Hanzo L. Soft-decision star-QAM aided BICM-ID. *IEEE Signal Processing Letters* 2011; **18**(3): 169–172.
20. Xu C, Liang D, Ng SX, Hanzo L. Reduced-complexity noncoherent soft-decision-aided DAPSK dispensing with channel estimation. *IEEE Transactions on Vehicular Technology* 2013; **62**(6): 2633–2643.
21. Lott M. Comparision of frequency and time domain differential modulation in an OFDM system for wireless ATM. In *IEEE Vehicular Technology Conference*, Vol. 2, Amesterdam, July 1999; 877–883.
22. Lijun S, Youxi T, Shaoqian L, Yingtao L. BER performance of differential demodulation OFDM system in multipath fading channels. In *IEEE GLOBECOM*, Vol. 1, San Francisco, USA, December 2003; 1–5.
23. *Evolved Universal Terrestrial Radio Access (E-UTRA); Physical layer procedures*, 3GPP TS 36.213 V8.8.0, Release 8, (2009-10).
24. *Evolved Universal Terrestrial Radio Access (E-UTRA); Further advancements for E-UTRA physical layer aspects*, 3GPP TR 36.814, V9.0.0 (2012-03), Release 9.

AUTHORS' BIOGRAPHIES

Imen Mrissa was born in Tunis, Tunisia. She received the Engineering Diploma in Telecommunications from the École Nationale d'Ingénieurs de Tunis (ENIT), Tunisia, in 2006 and the M.Sc. and Ph.D. degrees in telecommunications from INRS-EMT, Université du Québec, Montreal, Canada, in 2009 and 2016, respectively. Her research focuses on channel estimation, data demodulation, cognitive transceiver designs, LTE, HetNet, and both link- and system-level simulations. She received for both her M.Sc. and Ph.D. programs the National Grant of Excellence from the Tunisian Government. She was selected to receive a scholarship from the NSERC CREATE PERSWADE Program for the year 2015.

Faouzi Bellili was born in Tunisia on June 16, 1983. He received the B.Eng. degree (with Hons.) in signals and systems from the Tunisia Polytechnic School in June 2007, and the M.Sc. and Ph.D. degrees (both with the highest honours) from the National Institute of Scientific Research (INRS-EMT), University of Quebec, Montreal, QC, Canada, in December 2009 and August 2014, respectively. He is currently working as a Research Associate at INRS-EMT. In February 2016, he was awarded a PDF Grant from NSERC for a two-year tenure at the University of Toronto starting in September 2016. Dr. Bellili's research focuses on statistical signal processing and array processing with an emphasis on parameters estimation for wireless communications. He authored/co-authored over 40 peer-reviewed papers in reputable IEEE journals and conferences. He was selected by INRS as its candidate for the 2009–2010 competition of the very prestigious Vanier Canada Graduate Scholarships program. He also received the Academic Gold Medal of the Governor General of Canada for the year 2009–2010 and the Excellence Grant of the Director General of INRS for the year 2009–2010. He also received the award of the best M.Sc. thesis of INRS-EMT for the year 2009–2010 and twice — for both the M.Sc. and Ph.D. programs — the National Grant of Excellence from the Tunisian Government. He was awarded in 2011 the Merit Scholarship for Foreign Students from the Ministère de l'Éducation, du Loisir et du Sport (MELS) of Québec, Canada. Dr. Bellili recently served as TPC member for IEEE GLOBECOM and IEEE ICUWB and regularly acts as a reviewer for many international scientific journals and conferences.

Sofiène Affes received the Diplôme d'Ingénieur in telecommunications, and the Ph.D. degree (Hons.) in signal processing, from École Nationale Supérieure des Télécommunications (ENST), Paris, France, in 1992 and 1995, respectively. He was a Research Associate with INRS, Montreal, QC, Canada, until 1997, an Assistant Professor, until 2000, and an Associate Professor, until 2009. Currently, he is a Full Professor and Director of PERWADE, a unique 4M$ research training program on wireless in Canada involving 27 faculty from eight universities and ten industrial partners. From 2003 to 2013, he was a Canada Research Chair in wireless communications. In 2006 and 2015, he served as a General Co-Chair of IEEE VTC'2006-Fall and IEEE ICUWB'2015, respectively, both held in Montreal, QC, Canada. He will act as General Chair of IEEE PIMRC'2017 to be held in Montreal, QC, Canada. Currently, he is an Associate Editor for the IEEE TRANSACTIONS ON COMMUNICATIONS and the Wiley Journal on Wireless Communications and Mobile Computing. He was an Associate Editor for the IEEE TRANSACTIONS ON WIRELESS COMMUNICATIONS, from 2007 to 2013, and the IEEE TRANSACTIONS ON SIGNAL PROCESSING, from 2010 to 2014. He has been twice the recipient of a Discovery Accelerator Supplement Award from NSERC, from 2008 to 2011 and from 2013 to 2016. In 2008 and 2015, he received the IEEE VTC Chair Recognition Award from IEEE VTS and the IEEE ICUWB Chair Recognition Certificate from IEEE MTT-S for exemplary contributions to the success of IEEE VTC and IEEE ICUWB, respectively.

Alex Stéphenne was born in Quebec, Canada, on May 8, 1969. He received the B.Ing. degree in electrical engineering from McGill University, Montreal, Quebec, in 1992, and the M.Sc. degree and Ph.D. degrees in telecommunications from INRS-Télécommunications, Université du Québec, Montreal, in 1994 and 2000, respectively. In 1999 he joined SITA Inc., in Montreal, where he worked on the design of remote management strategies for the computer systems of airline companies. In 2000, he became a DSP Design Specialist for Dataradio Inc. (now part of CalAmp), Montreal, a company specializing in the design and manufacturing of advanced wireless data products and systems for mission critical applications. In January 2001 he joined Ericsson and worked for over two years in Sweden, where he was responsible for the design of baseband algorithms for WCDMA commercial base station receivers. From 2003 to 2008, he is still working for Ericsson, but is now based in Montreal, where he is a researcher focusing on issues related to the physical layer of wireless communication systems. From 2009 to 2014, he is a researcher for Huawei, in Ottawa, working on radio resource management for 4G and 5G systems. Since 2014, he is with Ericsson in Ottawa, as a wireless system designer. He is also an adjunct professor at INRS since 2004 and a Senior member of the IEEE.

DOI: 10.1002/wcm